





Open conformation of tetraspanins shapes interaction partner networks on cell membranes

Yihu Yang¹, Xiaoran Roger Liu² , Zev J Greenberg³, Fengbo Zhou¹, Peng He¹, Lingling Fan¹, Shixuan Liu¹ , Guomin Shen¹ , Takeshi Egawa⁴, Michael L Gross², Laura G Schuettelpelz³ & Weikai Li^{1,*} 

Abstract

Tetraspanins, including CD53 and CD81, regulate a multitude of cellular processes through organizing an interaction network on cell membranes. Here, we report the crystal structure of CD53 in an open conformation poised for partner interaction. The large extracellular domain (EC2) of CD53 protrudes away from the membrane surface and exposes a variable region, which is identified by hydrogen–deuterium exchange as the common interface for CD53 and CD81 to bind partners. The EC2 orientation in CD53 is supported by an extracellular loop (EC1). At the closed conformation of CD81, however, EC2 disengages from EC1 and rotates toward the membrane, thereby preventing partner interaction. Structural simulation shows that EC1–EC2 interaction also supports the open conformation of CD81. Disrupting this interaction in CD81 impairs the accurate glycosylation of its CD19 partner, the target for leukemia immunotherapies. Moreover, EC1 mutations in CD53 prevent the chemotaxis of pre-B cells toward a chemokine that supports B-cell trafficking and homing within the bone marrow, a major CD53 function identified here. Overall, an open conformation is required for tetraspanin–partner interactions to support myriad cellular processes.

Keywords CD19; CD53; CD81; cell migration; tetraspanin

Subject Categories Cell Adhesion, Polarity & Cytoskeleton; Structural Biology

DOI 10.15252/emboj.2020105246 | Received 10 April 2020 | Revised 8 July 2020 | Accepted 13 July 2020 | Published online 16 August 2020

The EMBO Journal (2020) 39: e105246

Introduction

Tetraspanins participate in a wide array of cellular processes including cell proliferation, migration, adhesion, fusion, and signaling (Termini & Gillette, 2017; Yeung *et al.*, 2018). There are 33 tetraspanin members identified in the human genome. The well-studied

CD81 is required for sperm–egg fusion during the fertilization process (Sutovsky, 2009), for cell composition regulation in the central nervous system (Geisert *et al.*, 2002; Charrin *et al.*, 2009), and for maturation of CD19 (Maecker & Levy, 1997; Shoham *et al.*, 2003, 2006; Bagashev *et al.*, 2018), a major immunotherapy target against lymphoma and leukemia (Park *et al.*, 2016; Braig *et al.*, 2017; Velasquez & Gottschalk, 2017). Most tetraspanins, including CD81, are widely distributed in cells and tissues. As an exception, CD53 is expressed exclusively in leukocytes. CD53 is involved in B-cell differentiation and modulation of inflammatory responses (Beckwith *et al.*, 2015; Zuidschouwde *et al.*, 2017; Greenberg *et al.*, 2020). Familial deficiency of CD53 expression manifests as recurrent infections (Mollinedo *et al.*, 1997), whereas increased CD53 expression correlates with the active status of tuberculosis patients (Omae *et al.*, 2017). Overall, these examples highlight the essential functions of tetraspanins under physiological and pathological conditions.

Tetraspanins facilitate these cellular processes through organizing molecules at the plasma membrane, thereby generating a hierarchical interaction network (Charrin *et al.*, 2014). Tetraspanins interact with each other and with a large repertoire of partners, many of which contain immunoglobulin-like (Ig) domains. The partner interactions are primarily through a large extracellular domain (EC2), which contains a variable region that may control the partner-interaction specificity such as CD81 with CD19 (Shoham *et al.*, 2006) and CD53 with CD2 (Bell *et al.*, 1992). Owing to this functional importance, the structural patterns of EC2 have been used to classify tetraspanins (Seigneuret *et al.*, 2001). A small extracellular loop (EC1) in tetraspanins is also highly variable, but its functional role remains elusive (Van Deventer *et al.*, 2017). Among the proteins with four transmembrane helices (TM), tetraspanins are distinguished by the unequal size of EC1 and EC2 and by the cysteine pattern of EC2, which contains two to four cysteine pairs including a CCG motif (Huang *et al.*, 2005). The transmembrane region of tetraspanins is also involved in partner interactions; for example, TM1 of CD81 supports the exit of CD19 from the endoplasmic reticulum (Shoham *et al.*, 2006). The two termini of tetraspanins are located at the cytosolic side, providing additional interaction sites

1 Department of Biochemistry and Molecular Biophysics, Washington University School of Medicine, St. Louis, MO, USA

2 Department of Chemistry, Washington University, St. Louis, MO, USA

3 Division of Hematology and Oncology, Department of Pediatrics, Washington University School of Medicine, St. Louis, MO, USA

4 Department of Pediatrics Pathology and Immunology, Washington University School of Medicine, St. Louis, MO, USA

*Corresponding author. Tel: +1 314 362 8687; E-mail: weikai@wustl.edu

for signaling molecules (Van Deventer *et al*, 2017). As an example, the N-terminal of CD53 interacts with PKC- β to regulate B-cell signaling (Zuidischerwoude *et al*, 2017). Taken together, multiple structural regions of tetraspanins are required to organize their partner interactions (Van Deventer *et al*, 2017). The molecular nature of these organizations and their regulation of cellular responses, however, remain largely unknown.

In the entire tetraspanin superfamily, the full-length structure is known only for human CD81 and CD9 (reported during the submission of this manuscript), both captured in a closed conformation incapable of partner interactions (Zimmerman *et al*, 2016; Umeda *et al*, 2020). The four TMs of CD81 and CD9 form a cone-shaped structure that splits into two TM pairs at the extracellular side. The EC2 domain of CD81 adopts a mushroom-like structure with five helices (named A to E); the A and E helices form the mushroom “stalk”, and B and variable C–D region form the “head”. The isolated EC2 domain of CD81 shows essentially the same structure (Kitadokoro *et al*, 2001), and the mushroom fold is observed also in the CD9 structure and in the NMR structure of the EC2 domain of another tetraspanin, TSP-2, from *Schistosoma mansoni* (Jia *et al*, 2014). The EC1 loop, the loop connecting TM2 and TM3 (L2–3), and part of the N- and C-termini, however, are disordered in the full-length CD81 structure, the resolution of which is compromised by anisotropic crystal diffraction (5.5 and 2.95 Å). Nevertheless, the electron densities of this structure suggest that a cholesterol molecule is bound at the transmembrane region, and molecular dynamics simulation implies that cholesterol dissociation changes the structure of the transmembrane domain to induce the open conformation. Despite such modeling attempts (Zimmerman *et al*, 2016; Umeda *et al*, 2020), a tetraspanin structure at the partner-interactive state is required to understand the molecular mechanism regulating the tetraspanin network.

Here, we report the 2.9 Å structure of CD53 in the open conformation. Unexpectedly, the transmembrane domain of CD53 without bound cholesterol adopts essentially the same structure as the closed conformation of CD81. EC2 of CD53, however, rotates to a different angle owing to supporting interactions from EC1. After the rotation, the EC2 variable region is exposed for partner binding at the open conformation. In contrast, this region faces the membrane surface and is partially buried in the closed conformation of CD81. Hydrogen–deuterium exchange mass spectrometry (HDX-MS) shows that CD53 and CD81 use a similar part of their variable region to interact with extracellular domains of their partners, CD2 and CD19, respectively. Mutations that disrupt the EC1-EC2 interface of CD81 interfere with its ability to promote accurate glycosylation of CD19. Similar mutations in CD53 interfere with B-cell migration, which we identify to be a major cellular function of CD53. Thus, the open and closed conformational changes may regulate partner interactions of tetraspanins in a wide range of cellular processes.

Results

CD53 structure

Human CD53 was crystallized in lipid cubic phase (LCP), and the crystals diffracted isotopically to 2.9 Å (Table 1) with a construct carrying an Asn148Ala mutation to eliminate a predicted

glycosylation site, and Cys80Ala and Cys208Ala mutations to prevent palmitoylation. The electron density map reveals nearly the entire structure of CD53 including the loop and termini regions (Fig EV1A). The CD53 molecules pack artificially into an antiparallel dimer in each asymmetric unit of the crystals (Fig EV1B); these two molecules face different packing interactions and yet their structures, including the termini tails, are nearly identical (Fig EV1C).

The four TMs of CD53 adopt a cone-shaped conformation (Fig 1A and B). At the cytoplasmic side, the TMs pack tightly into a bundle at an angle to each other. The packing primarily uses knob-

Table 1. Data collection, phasing, and refinement statistics.

Protein	CD53
Data collection^a	
Space group	$P2_1$
Solvent content (%)	67.0
Cell dimensions	
<i>a</i> , <i>b</i> , <i>c</i> (Å)	49.4, 210.5, 73.4
α , β , γ (°)	90, 100.2, 90
Resolution (Å)	50–2.9 (2.95–2.90) ^b
$CC_{1/2}$ ^c	0.998 (0.772)
R_{sym}	0.128 (0.738)
$I/\sigma I$	8.4 (1.4)
Completeness (%)	93.3 (97.2)
Redundancy	2.8 (2.8)
Refinement	
Resolution (Å)	50–2.9
No. reflections	24,301
$R_{\text{work}}/R_{\text{free}}$ ^d	22.3/26.5
No. atoms	
Protein	6,915
Ligand/ion	151
Water	19
<i>B</i> -factors (Å ²)	
Protein	60.9
Ligand/ion	55.4
Water	61.1
Ramachandran plot	
Favored (%)	97.4
Allowed (%)	2.6
Outliers (%)	0.0
R.m.s deviations	
Bond lengths (Å)	0.006
Bond angles (°)	0.952

^aThe dataset was derived from a single crystal.

^bValues in parentheses are for the highest-resolution shell.

^c $CC_{1/2}$ = Pearson correlation coefficient between random half-datasets.

^d $R_{\text{work}} = \sum h ||F_o(h)| - |F_c(h)|| / \sum h |F_o(h)|$, where $|F_o|$ and $|F_c|$ are the observed and calculated structure-factor amplitudes, respectively. R_{free} was calculated with 5% of the data excluded from the refinement.

and-hole interactions from the side chains in the TMs (Fig 1C), the region that human tetraspanins share high sequence similarity (Fig EV2). About halfway in the membrane, the TM1/TM2 and TM3/TM4 pairs start to split, creating a tunnel between TM1 and TM4 that is delineated by several hydrophobic residues (Fig 1B). Elongated electron densities were observed in this tunnel (Fig EV1A) and assigned to monoolein, a lipid used for the LCP crystallization. Further splitting of the TM pairs at the extracellular side leaves a large opening (Fig 1B), which affords a potential site designated for binding the transmembrane domain of interacting partners.

The EC2 domain of CD53 adopts a canonical mushroom fold (Fig 1D). The “stalk” helices A and E are connected to TM3 and

TM4, respectively. Both connections are through short hinges and with sharp bends. The two hinges are associated with each other through hydrophobic residues (Fig 2D). The interactions continue between the interface of helices A and E, involving stacking between hydrophobic residues and a hydrogen bonding network formed between polar residues. These extensive interactions stabilize the relative positions of the two stalk helices. CD53 lacks the helices C and D found in CD81 (Kitadokoro *et al*, 2001). This C–D region instead folds into two antiparallel loops, whose conformation is stabilized by the two disulfide bonds characteristic of tetraspanins. The EC2 head region, in particular the C–D region, is well exposed for interactions in the open conformation (Fig 1A).

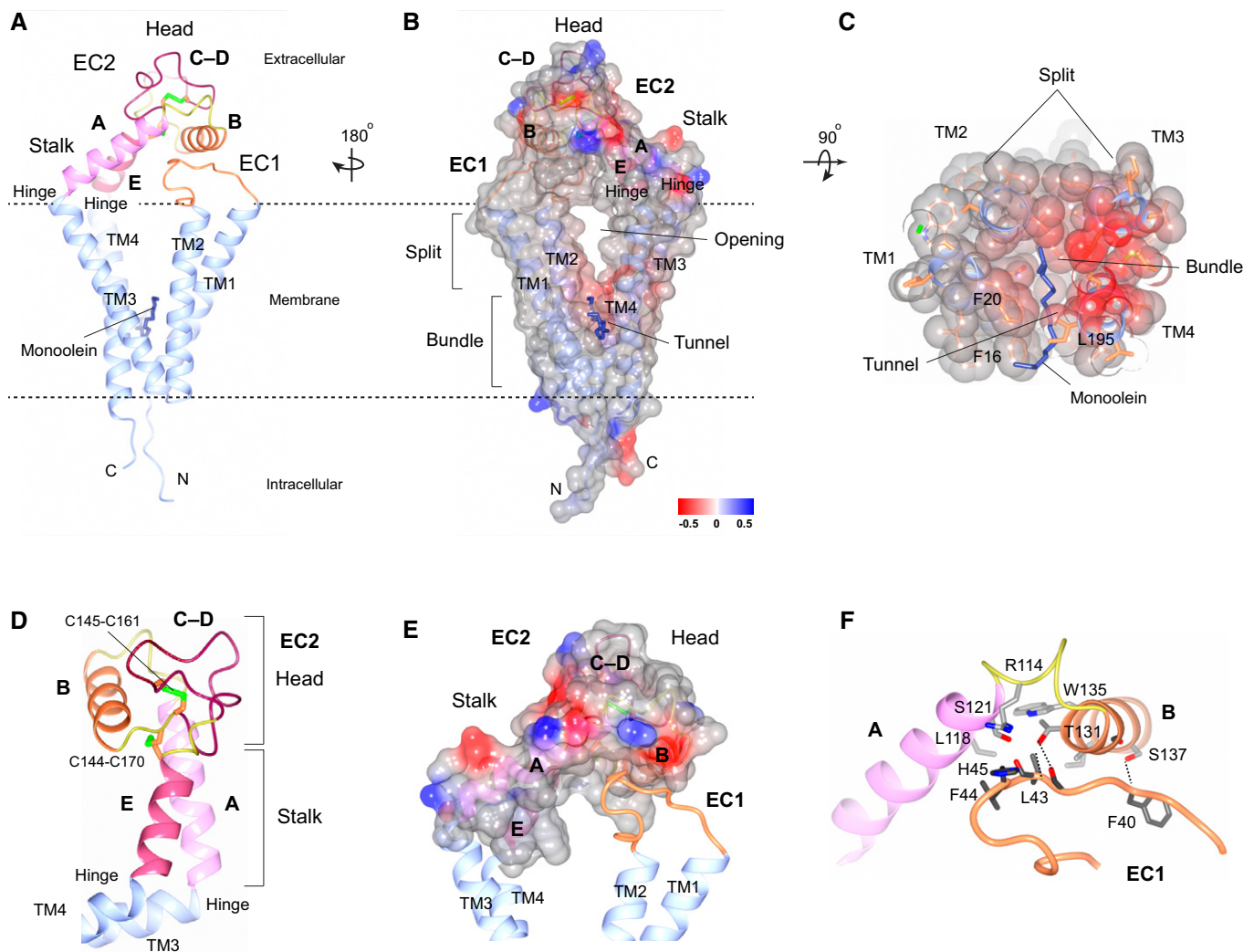


Figure 1. Structure of CD53 in the open conformation.

- A Overall structure (side view). EC1 and secondary structure elements in EC2 are shown in different colors, and the four TMs in blue.
 B Electrostatic surface representation of the structure (back view from A). The bundle region of TMs forms a tunnel that binds monoolein, and their splitting generates a lateral opening inside the membrane.
 C Van der Waals surface (top view) showing interactions between the TM1/2 and TM3/4 pairs near their splitting site and residues forming the lipid-binding tunnel.
 D Structure of the CD53 EC2 domain showing the mushroom fold with a head and stalk. The stalk helices connect to TM3 and TM4 through two hinges.
 E EC1 loop binds in the EC2 groove (electrostatic surface) formed by helices A and B.
 F Interactions stabilizing the EC1-EC2 binding.

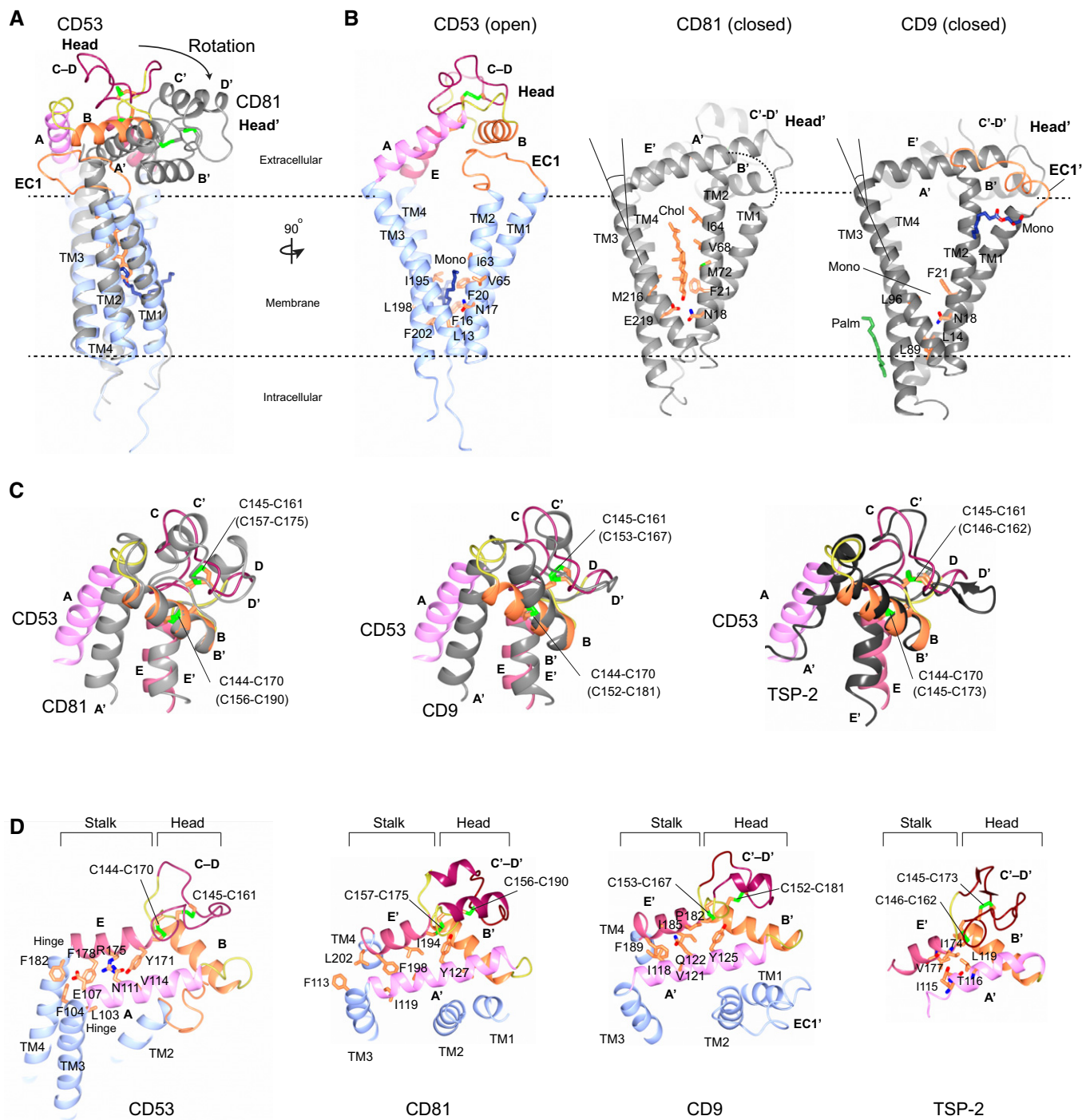


Figure 2. Structural comparison of CD53 in open conformation and CD81 and CD9 in closed conformation.

A Structures of CD53 (colored by structure elements) and CD81 (gray) superimposed by their transmembrane domains. The curved arrow indicates EC2 rotation. Letters with a prime sign (A'-E') indicate structural components of CD81.

B Comparison of individual structures of CD53 in open conformation (left), and CD81 (middle) and CD9 in closed conformation (right). The dashed curve indicates disordered EC1 in CD81, and the angles indicate bending of TM3 in CD81 and CD9. The bound cholesterol (Chol; orange) in CD81 and bound monoolein (Mono; blue) in CD53 and CD9 are indicated. CD9 structure contains palmitoylation sites (Palm, green) and another monoolein bound between the TM bundle. Since this monoolein molecule is not modeled in PDB 6K4J, we can only show surrounding residues here. Among these, Leu14, Asn18, and Phe21 are conserved between CD9, CD81, and CD53.

C EC2 domain structure of CD53 superimposed with those of CD81, CD9, and TSP2. The comparisons show the same position of two characteristic disulfide bonds and show differences in the C-D conformation and A-helix orientation.

D Interactions within the EC2 domains of CD53, CD81, CD9, and TSP-2. Relative orientation of the stalk helices and bending at the hinges are stabilized by extensive side-chain interactions. Folding of the head region is maintained by the two characteristic disulfide bonds.

This exposed orientation of EC2 is supported by its interaction with EC1. The central part of EC1 (residues 43–47) binds in a small groove of EC2 that is formed between helices A and B (Fig 1E). The side chains of Leu43 and Phe44 insert into the hydrophobic part of groove, and other interactions involve Phe40, His45, and backbone carbonyls of EC1 (Fig 1F). Owing to these stable binding interactions, EC1 is well ordered in the CD53 structure. With the support from EC1, EC2 is disengaged from the transmembrane domain (Fig 1E). Consequently, the head region of EC2 moves away from the membrane and sticks out into the extracellular space (Fig 1A). Thus, the head region is nearly free from steric hindrance and physically poised for partner interactions.

At the cytoplasmic side of the CD53 molecule, an interaction “cage” is formed between the loop connecting TM2 and TM3 (L2–3) and the N- and C-terminal tails (Fig EV3). Glu77 in L2–3 forms salt bridges with Lys7 and Lys10 at the N-terminus. These highly conserved Lys residues have been identified as ubiquitination sites in CD81, CD151, and TSPAN6 (Termini & Gillette, 2017), and their structural organization may have regulative roles.

Open and closed conformations

Structural comparison of CD53 and CD81 shows a large rotation between their EC2 and transmembrane domains (Fig 2A). With support by interactions from EC1, the EC2 head region of CD53 is twisted away from the membrane and exposed for interactions. In contrast, the EC1 loop of CD81 is disordered in the structure, and its EC2 instead interacts with TM1 and TM2 (Fig 2B). Similarly, EC2 interacts with the TM regions in the CD9 structure; although the EC1 loop is ordered in this structure, it flips to another side without forming interaction with EC2 (Fig 2B). Without the EC1 support, EC2 rotates to a different angle with its head region oriented toward the membrane, thereby generating a closed conformation in the CD9 and CD81 structures.

The relative rotation between EC2 and transmembrane domains can be regarded as a rigid-body movement because each individual domain adopts a similar conformation. In particular, the transmembrane domains of CD53 and CD81 are nearly superimposable (Fig 2A), with a 1.2 Å RMSD between their C_α atoms. The same cone-shaped conformation suggests that this is a canonical fold shared by all tetraspanins in their transmembrane domain. Despite the overall structural similarity, the TM2 of CD81 is one turn longer than that of CD53. Moreover, the TM3 of CD81 is bent by approximately 18° at the extracellular end, whereas the TM3 of CD53 is straight (Fig 2B). The CD9 structure shows a similar bending in TM3. The different conformations of TM3 are probably associated with the relative movement of EC2.

The transmembrane domains of these tetraspanins, at essentially the same conformation, form different lipid-binding sites (Fig 2B). In CD53, monoolein is bound in a tunnel that is formed by hydrophobic residues at the bottom part of the TM splitting. In CD9, a monoolein molecule is bound at a similar position that is surrounded by residues conserved between CD9, CD53 and CD81. In contrast, cholesterol is bound at an open pocket in CD81 and occupies a much larger area. At the bottom part of the TM splitting, the cholesterol hydroxyl group form hydrogen bonds with Asn18 in TM1 and Glu219 in TM4, and the cholesterol ring interacts with hydrophobic residues from all four TMs of CD81. After the TMs are

split, however, the other part of the cholesterol molecule interacts only along TM2. Importantly, the cholesterol binding after the splitting does not involve TM3 and TM4. Given that EC2 connects only to TM3 and TM4, it is unlikely that binding or dissociation of cholesterol induces EC2 rotation. Instead, the role of the lipids is probably to stabilize folding of the transmembrane domain.

The EC2 domains of different tetraspanins share the overall mushroom fold but with large structural deviations (Fig 2C). The C–D region of CD81 forms two helices in crystal structures, and the molecular shape of the head region differs from that of CD53 head. In CD9, the C region maintains a helical conformation, but the D region becomes a loop. On the other hand, the C–D regions of CD53 and TSP-2 form two loops that swing to different angles. These structural variations in the C–D region, along with sequence differences, may afford the specificity of partner recognition for different tetraspanins.

Folding of these variable regions is reinforced by two disulfide bonds conserved in the tetraspanin family. Remarkably, these disulfides are nearly superimposable in all four structures (Fig 2C and D). In addition, the E helix and at least part of the B helix can be closely superimposed. Helix A adopts different angles in these structures, however, owing to its different but extensive side-chain interactions with B and E (Fig 2D). Given that the sequence of helix A is poorly conserved (Fig EV2), this helix may change angles in different tetraspanins and alter their EC2 orientation in both open and closed conformations.

Mapping of tetraspanin–partner binding interfaces

To understand how the open and closed conformations affect the partner interactions of tetraspanins, we mapped the partner-binding interfaces of CD53 and CD81 by using HDX-MS. CD53 physically associates with CD2 (Bell *et al*, 1992), a membrane-anchored NK- and T-cell marker that contains two extracellular Ig domains. The association is likely through the EC2 domain of CD53 and two Ig domains of CD2, similar to other tetraspanin–partner interactions (Van Deventer *et al*, 2017). To characterize the binding interface, we purified the CD53 EC2 domain and CD2 Ig domains and conducted HDX-MS for the unbound and bound proteins. Comparison of the HDX kinetic curves shows that CD53 EC2 domain and CD2 Ig domains each have a single region that, upon binding, exhibits significant decreases in deuterium uptake with cumulative differences greater than three times of propagated error (99.7% confidence that differences are significant) (Figs 3A and B, and EV4A and B). In CD53 EC2, the protection seen in HDX corresponds to residues ¹⁵³WTSGPPASCPD¹⁶⁴ in the variable C–D region (Fig 3A). The protection in CD2 Ig domains is observed for two peptides (Fig EV4B), and their overlap indicates a binding region of ¹²⁴LKIQE¹²⁸ that is located at the joint between the two Ig domains (Fig 3C). The protection is observed to be nearly constant throughout the entire time of HDX (30 s to 4 h), suggesting a slow off rate for EC2 and Ig domains. Overall, HDX-MS reveals that the C–D region of CD53 binds to the Ig joint region of CD2 (Fig 3C).

Similarly, we conducted HDX-MS between the EC2 domain of CD81 and two Ig domains of CD19 (Figs 3D and EV4C and D). In CD81, multiple peptides show decreases in HDX upon interacting with CD19. These peptides overlap at residues ¹⁷¹KNNLCPSGSNIISNL¹⁸⁵ at the D-helix and its preceding loop, a region

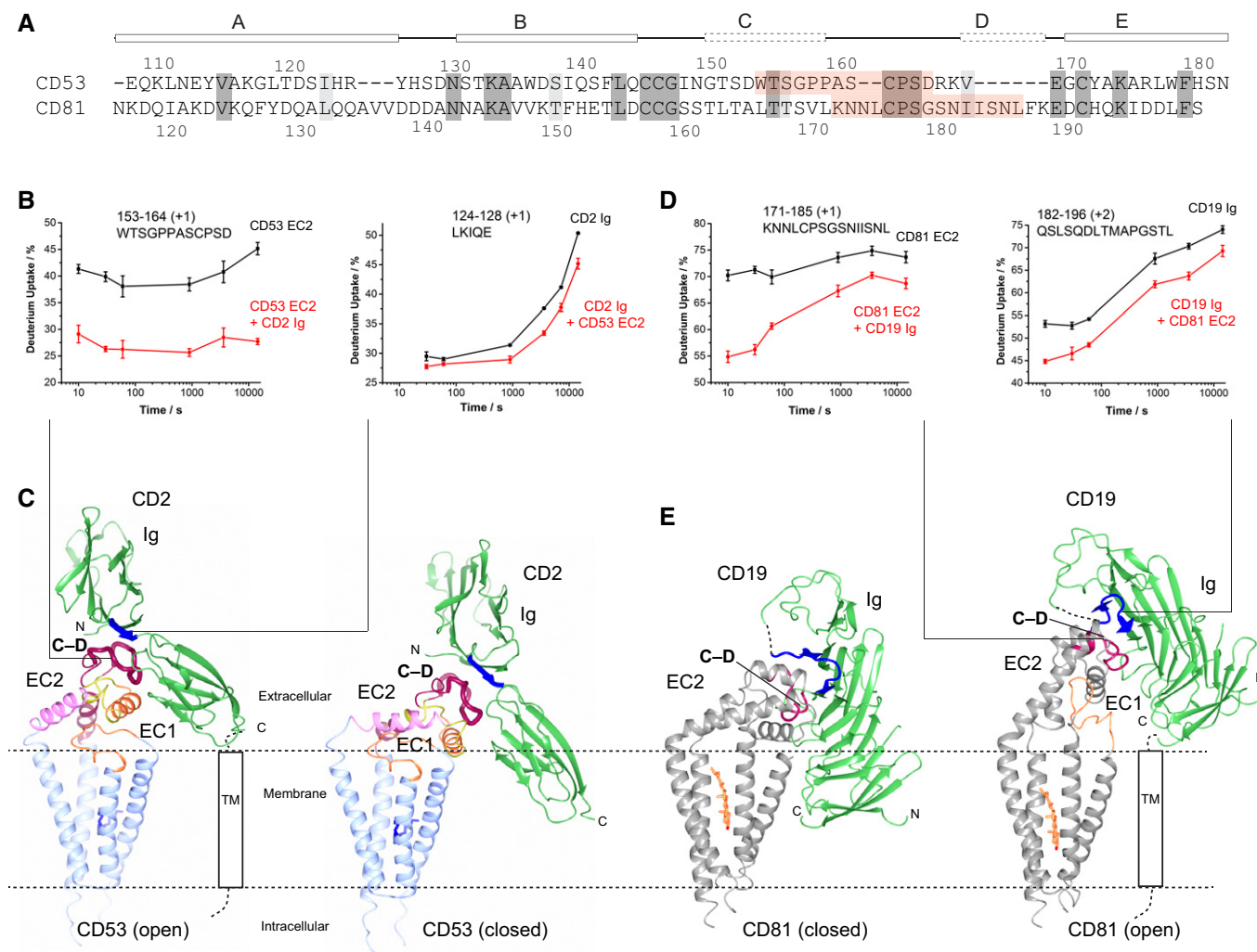


Figure 3. CD53-CD2 and CD81-CD19 partner interactions identified by HDX-MS and modeled onto open and closed conformations.

A The partner-binding regions of CD53 and CD81. Their EC2 sequences are aligned. Identical residues are shaded in dark gray, similar residues in light gray, and partner-binding regions identified by HDX-MS in orange. Secondary structures are indicated above.

B Representative HDX-MS curves showing the protected regions in CD53 and CD2. Other curves at these regions are shown in Fig EV4A and B, and complete HDX-MS results in Fig 3 Source Data. The HDX experiments were performed (manually or with a LEAP automation system) in triplicate. Error bars show the standard deviation.

C *Left*, CD53-CD2 docking model. The HDX-MS identified regions are shown as a red rod in CD53 and as a blue arrow in CD2. The black box indicates the CD2 transmembrane region, and the dashed line indicates the linker to Ig domains. *Right*, CD53-CD2 docking model with CD53 modeled in the closed conformation. The modeling was based on the CD81 structure, in which EC2 reorients to interact with the TM domain. Docking of CD19 Ig to CD53 EC2 is in the same manner as *Left*.

D Representative HDX-MS curves showing the protected regions in CD81 and CD19. Other curves at these regions are shown in Fig EV4C and D, and complete HDX-MS results in Fig 3 Source Data. The HDX experiments were manually performed in triplicate. Error bars show the standard deviation.

E *Left*, CD81-CD19 docking model in the closed conformation. The HDX-MS identified binding regions are colored as in **C**. *Right*, Modeled open conformation of CD81 and docking with CD19 (in the same manner as *Left*). MD simulation (1 μ s) of this open conformation is shown in Fig 4 and Movie EV1.

Source data are available online for this figure.

remarkably similar to that found in CD53 (Fig 3A). At the partner side, several peptides in CD19 Ig domains exhibit decreased deuterium uptake upon binding with CD81 EC2. These peptides overlap at residues ¹⁸²QLSQDLTMAPGSTL¹⁹⁶. Although the sequence coverage of CD19 is not 100%, most regions not covered are heavily glycosylated, making them unlikely to be part of the binding site. The only binding site (i.e., 182–196) we detected in CD19 is located at a distance from its membrane anchor domain

(Fig 3E). To access this binding site, the CD81 EC2 needs to protrude at sufficient height over the membrane plane (Fig 3E).

Tetraspanin–partner interaction at open and closed conformations

Based on the binding interfaces identified by HDX-MS, we generated a docking model between the crystal structures of CD53 (Fig 1A)

and CD2 Ig domains (PDB code 1HNF). The model shows that the EC2 C–D region inserts into a groove at the joint region of two Ig domains (Fig 3C). Besides the region identified by HDX-MS, the docking model suggests that the stable binding requires additional interactions between the C–D region on EC2 and the C-terminal Ig domain, which is located just above the membrane and well positioned to connect with the transmembrane region of CD2. Importantly, the joint connecting the two Ig domains and the CD53 C–D region are positioned at the same height above the membrane plane for binding to occur. This height-matching requirement may contribute to the partner specificity of different tetraspanins.

Similarly, an HDX-based docking model can be created between the crystal structures of the CD81 (PDB code 5TCX) and CD19 Ig domains (PDB code 6AL5). The model shows that the binding results in a severe clash between the CD19 Ig domains and the membrane plane (Fig 3E). Thus, the closed conformation prevents CD81 from partner interactions, as was previously proposed (Zimmerman *et al*, 2016). Modeling of CD53 in a closed conformation shows a similar scenario (Fig 3C). In the absence of EC1 support, EC2 rotates toward the membrane and lowers the above-membrane height of the C–D variable region. Consequently, CD2 binding via this variable region results in a severe clash with the plasma membrane, thereby preventing the partner interaction.

To understand how CD81 interacts with its partner, we modeled the open conformation of CD81 on the basis of the CD53 structure, in which the exposed orientation of EC2 is back supported by its interaction with EC1 (Fig 1A). The central region of CD81 EC1 contains a short hydrophobic segment (LLYL) as CD53 EC1 does (Fig EV2C). Moreover, the A, B, and E helices of CD81 form a hydrophobic groove that is conserved between most tetraspanins (Seigneuret, 2006). Thus, we could build an open conformation model of CD81 in which its EC2 groove binds the LLYL segment (Fig 3E). Compared to CD53, the EC1 loop of CD81 is longer, and its A-helix adopts a different orientation (Fig 2C). Thus, the CD81 model suggests that its EC2 protrudes higher from the membrane plane (Fig 4A). Consequently, the bound CD19 Ig domains are placed well above the membrane plane (Fig 3E), avoiding the clashes observed in the closed conformation.

To assess the stability of this open conformation, we performed molecular dynamics simulation of CD81 in absence of a bound cholesterol. During the 1 μ s simulation time, the transmembrane domain of CD81 undergoes only slight motions and essentially maintains the same conformation shared by the CD81 and CD53 crystal structures (Fig 4A and B; Movie EV1). Furthermore, EC2 retains the open conformation due to the supporting interactions from EC1. The stable EC1–EC2 interaction hinders not only the EC2 rotation but also the relative movement between the TM1/2 and TM3/4 pairs. With such mutual stabilization, conformations of the transmembrane and EC2 domains are nearly unaffected by the binding or release of cholesterol. In addition, our modeling shows that helices A, B, and E from CD81 EC2 retain their alpha helical structure, whereas helices C and D are much more mobile and tend to lose their helical conformation during the MD simulation (Fig 4C). This structural conversion is consistent with the observations that the D region is helical in the crystal structures (Kitadokoro *et al*, 2001; Zimmerman *et al*, 2016) but is disordered in the solution NMR structure (Rajesh *et al*, 2012). This variable C–D region,

however, could be conformationally stabilized upon binding to the CD19 Ig domains (Fig 3E).

Accurate glycosylation of CD19 requires CD81 at the open conformation

The structural results suggest that an open conformation of CD81 is required for partner interaction. As a prominent example, CD81 facilitates the trafficking and processing of CD19 and stabilizes CD19 on the cell surface (Shoham *et al*, 2006; Bagashev *et al*, 2018). To investigate this CD19 maturation process, we constructed a CD81-knockout 293T cell line (Fig 5A) to avoid the interference from high level of endogenous CD81 in 293T. CD19, on the other hand, is exclusively expressed in lymphoid cells and not in 293T (Wang *et al*, 2012). CD19 transfection into the CD81-knockout cells generated three CD19 forms (Fig 5B, lane 1), similar to those observed in an early B-lineage cell line (Shoham *et al*, 2006). The low MW band is known as the precursor form of CD19 (pCD19) because it is in the endoplasmic reticulum (or pre-Golgi) and has a low glycosylation extent. Consistently, pCD19 is sensitive to Endo-H digestion (Fig 5B, lane 5). In contrast, two higher MW species, known as the mature forms (mCD19 and m'CD19), are Endo-H-resistant, indicating that complex oligosaccharide addition occurs after CD19 is trafficked through Golgi. PNGase F deglycosylation of mCD19, m'CD19, and pCD19 generated protein bands of the same MW (Fig 5B, lanes 3 and 4), indicating that these species differ only in their glycosylation content. Unlike pCD19, mCD19 and m'CD19 are sensitive to trypsin digestion of the intact cells (Fig 5C, lane 3), indicating their location on the cell surface. Previous studies show that mCD19 is the functional form of CD19 and m'CD19 is an overglycosylated form (Shoham *et al*, 2006).

In absence of CD81, the mCD19 and m'CD19 levels are similar, and they are lower than the pCD19 level (Fig 5B, lane 1). In contrast, CD81 transfection drastically increased the mCD19 level and generated multiple bands with the same and lower MW (Fig 5B, lane 2). Moreover, m'CD19 disappears in presence of CD81. Thus, CD81 plays two major roles during CD19 maturation: generating more CD19 on the cell surface and ensuring its accurate glycosylation, consistent with previous reports (Shoham *et al*, 2006; Bagashev *et al*, 2018).

This assay system allowed the investigation of CD81 mutants disrupting the open conformation. According to our structural model, the CD81 open conformation is stabilized by EC1–EC2 interactions that use a group of hydrophobic residues (Leu44, Leu45, Tyr46, and Leu47) in the center of EC1 loop (Fig 5D). Thus, we made a multi-alanine mutant (44A/45A/46A/47A; named A4) and also mutated each of these hydrophobic residues to glutamate (44E, 45E, 46E, 47E). Compared to the wild-type CD81 (Fig 5E, lane 2), the A4 mutant clearly alters the glycosylation pattern of CD19: The m'CD19 band appears, and mCD19 shifts to higher MW bands (Fig 5E, lane 3). The single mutants show less drastic effects, but they also alter the CD19 glycosylation to various extents (Fig 5E, lanes 4–7; repeat experiments in Fig EV5). We also made Glu219Ala and Glu219Gln substitutions to disrupt the cholesterol-binding site in CD81; cholesterol dissociation was suggested to induce the open conformation and facilitate CD19 maturation (Zimmerman *et al*, 2016). However, we found that Glu219Ala interferes with the maturation process by increasing the m'CD19 level, whereas Glu219Gln

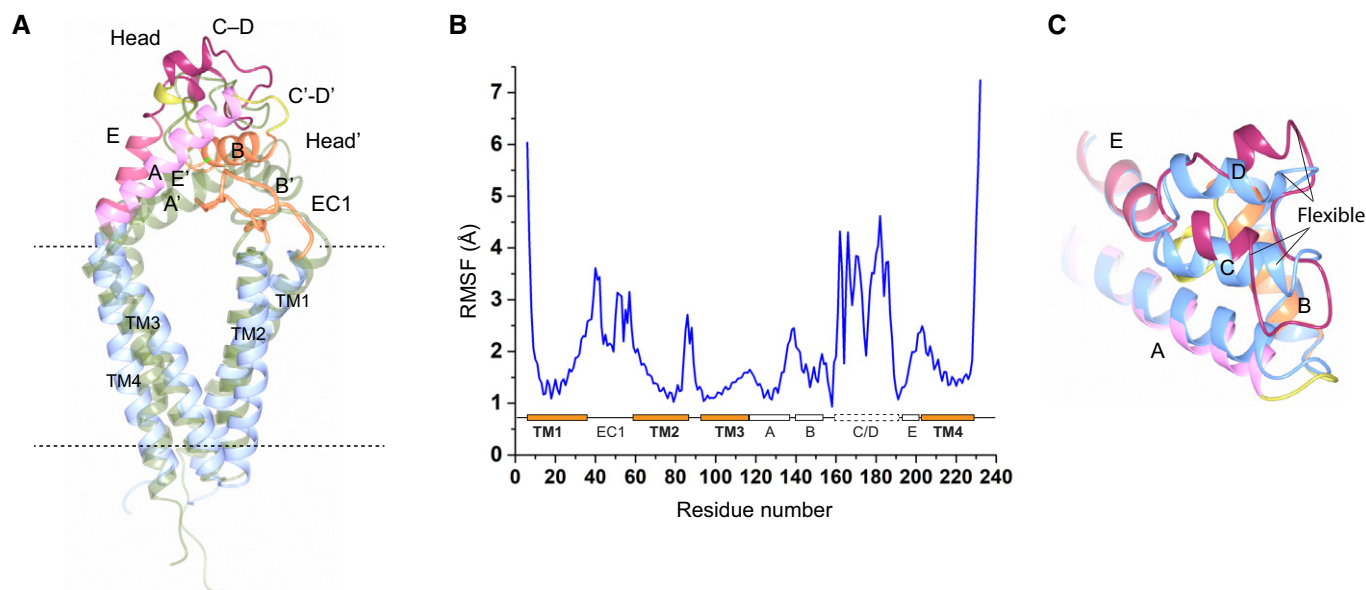


Figure 4. Molecular dynamics simulation of the CD81 open conformation.

- A** Comparison of the CD81 model (after 1 μ s simulation; colored by structural elements) and the CD53 crystal structure (green). Compared to CD53, the conformation of CD81 EC2 protrudes higher from membrane plane owing to the longer EC1 and different helix A orientation in CD81. The transmembrane regions of CD53 and CD81 are essentially unchanged during the 1 μ s simulation. The MD simulation is performed using GROMACS (Van Der Spoel *et al*, 2005) and CHARMM36m force field (Huang *et al*, 2017).
- B** RMSF plot shows motions of the TMs and EC2 during the MD simulation of CD81. The secondary structures are indicated below the curve. A, B, and E helices are relatively stable (< 2 Å) during the 1 μ s simulation time. In contrast, the C-D region is more flexible.
- C** Structural flexibility of CD81 C-D region. The EC2 domains of the CD81 MD model after 1 μ s simulation (colored by structural elements) and the CD81 crystal structure (blue) are superimposed.

shows little effect (Fig EV5B). These Glu219 mutants, as the EC1 mutants, do not affect the total level of mCD19 and m'CD19 by much, consistent with a later report using flow cytometry to show that the surface CD19 level is basically unchanged with Glu219 mutations (Palor *et al*). Taken together, cholesterol dissociation from CD81 may not induce its open conformation, consistent with our structural observations (Fig 2A and B). Instead, it is the EC1 support that stabilizes the open conformation of CD81, which is required for the proper glycosylation of CD19.

CD53-assisted B-cell migration

Many members of the tetraspanin family are important for immune cell trafficking, a process central to the immune system function (Yeung *et al*, 2018). Because CD53 is exclusively expressed in leukocytes, we investigated whether CD53 is required for the migration of these immune cells. To this end, we derived pre-B cells from the bone marrow of WT and Cd53^{-/-} mice. Indeed, we found that the Cd53^{-/-} pre-B cells had significantly impaired migration toward the CXCL12 (Fig 6A), a chemokine supporting B-cell trafficking and homing within the bone marrow (Möhle *et al*, 2000). To determine whether this disability of migration is due to lack of CD53, we performed rescue experiments by infecting Cd53^{-/-} cells with a retrovirus containing the mice CD53 cDNA. Remarkably, the retroviral-mediated expression of CD53 in Cd53^{-/-} pre-B cells rescued their ability to migrate toward CXCL12 (Fig 6B).

Because the crystal structure of CD53 shows that its open conformation requires the EC1 support, we next examined whether EC1 mutations in CD53 can affect the migration of pre-B cells. Similar to the design of CD81 EC1 mutations, we made a multi-alanine mutant (Leu43Ala/Phe44Ala/His45Ala/Asn46Ala, named A4) and single mutants of Leu43Glu and Phe44Glu in CD53; in the crystal structure, these EC1 residues bind directly at the small groove of EC2 (Fig 1E and F). Compared to wild-type CD53, all three mutants abolish the rescue of Cd53^{-/-} migration toward CXCL12, to a similar level as does Cd53^{-/-} (Fig 6B). Taken together, we find that a major function of CD53 is to support B-cell migration, consistent with a recent report that CD53 facilitates the homing of B and T cells to lymph nodes (Demaria *et al*, 2020). The EC1-EC2 interaction is necessary for this function, presumably by supporting the open conformation of CD53 that allows partner interaction.

Discussion

Tetraspanins promote a hierarchy of cellular processes through interacting specifically with multiple partners and organizing them on the cell membrane (Van Deventer *et al*, 2017). The crystal structure of CD53 reported here shows an open conformation capable of such partner interactions. Mutations disrupting the open conformation prevent CD53 from promoting B-cell migration (Fig 6B), although the CD53 partner involved in this process is unknown.

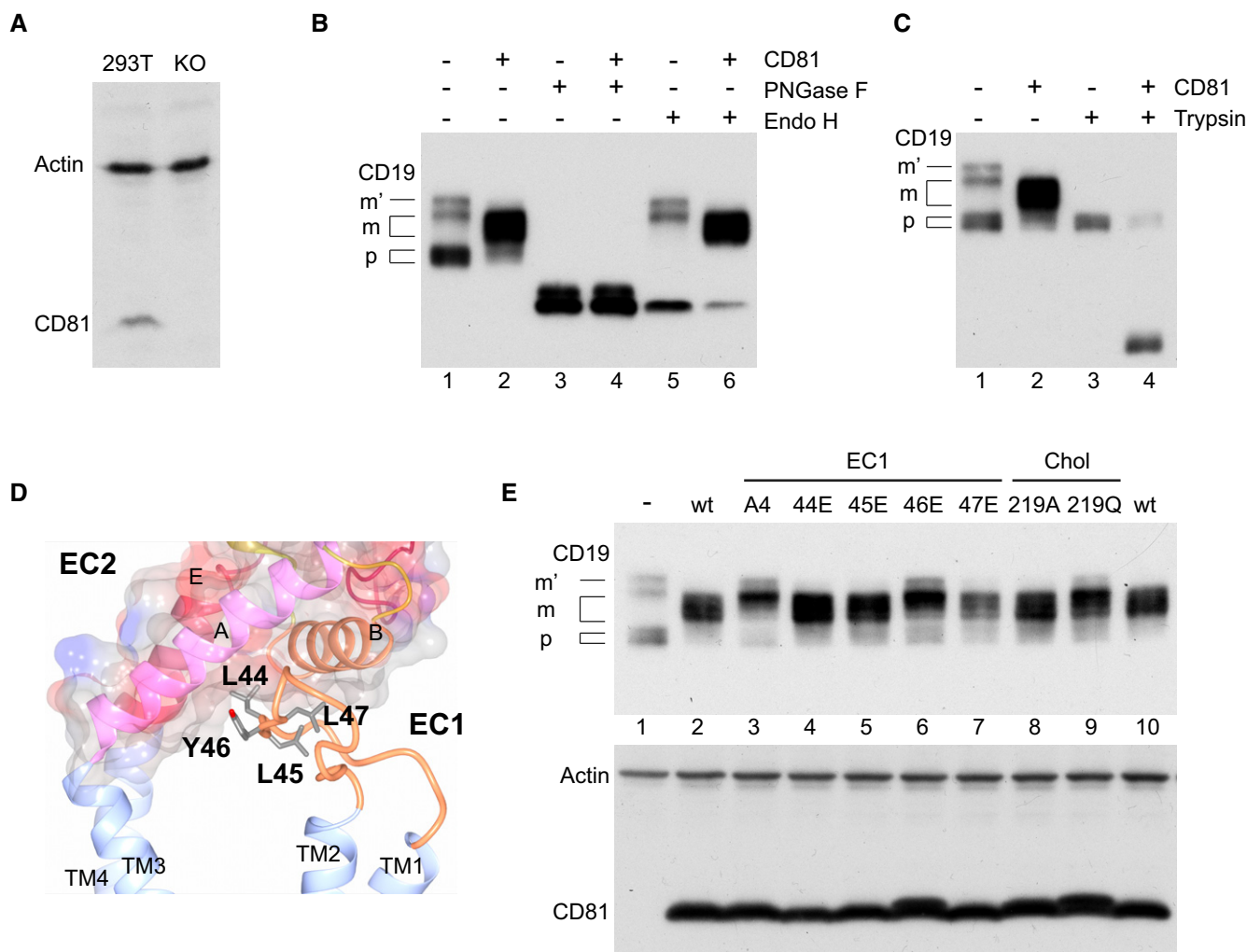


Figure 5. Accurate glycosylation of CD19 requires the EC1-supported conformation of CD81.

A CD81 knockout of 293T cells. The knockout cell line was generated by CRISPR-Cas9. The immunoblots using CD81 antibody and actin antibody were conducted on the same film.

B CD81 facilitates CD19 maturation. CD81 and CD19 (300 ng DNA) were transfected into the CD81-knockout 293T cells. Anti-FLAG immunoblot was performed for CD19 with a C-FLAG tag. The deglycosylation was performed by digesting the cell lysate with PNGase F or Endo H, following the manufacturers' instructions. The deglycosylation pattern of CD19 species (p: precursor, m and m': two mature forms) differs because the glycosylation content of these species is different (see text for explanation).

C Trypsin digestion of CD19. The digestion was performed at 37°C with intact cells. The mature CD19 forms (m and m') can be digested because they are surface expressed, whereas the intracellular precursor form (p) is protected from the digestion.

D EC1-EC2 interaction in the CD81 open conformation (modeled as in Fig 3E, right). The EC2 hydrophobic groove is shown in surface representation, and the interacting EC1 residues are indicated.

E EC1 mutants of CD81 interfere with the accurate glycosylation of CD19. Chol: mutations at the cholesterol-binding site of CD81. CD81 constructs and CD19 (300 ng DNA) were co-transfected into the CD81-knockout 293T cells. *Top*, Anti-FLAG immunoblot was performed for CD19 with a C-FLAG tag. In presence of wild-type CD81 (wt), most CD19 is in the properly glycosylated mature form (m), and the overglycosylated m' form is not observed. With the EC1 mutants (A4 in particular), however, m' emerges and m shifts to high MW, indicating an alteration in the CD19 glycosylation. The level of intracellular p form is low with the wild-type CD81 or with the mutants. *Bottom*, Control experiment showing similar expression level of wild-type CD81 and CD81 mutants. Anti-V5 immunoblotting was conducted for the CD81 constructs with a C-V5 tag, and anti-actin immunoblotting was conducted on the same film.

Similar mutations in CD81 hinder the accurate glycosylation of its CD19 partner, suggesting that the open conformation is also required for CD81 function; defective CD19 maturation, including misglycosylation, results in CD19 immune escape in CAR-T immunotherapy, a major resistance problem for patients with acute lymphoblastic leukemia (Fischer *et al*, 2017; Velasquez & Gottschalk, 2017). Taken together, the open conformation is critical

for different tetraspanin functions in cellular and therapeutic processes.

Structural comparison and the subsequent functional studies provide the experimental evidences that EC2 rotation controls partner interactions, consistent with predictions from previous MD simulations (Zimmerman *et al*, 2016; Umeda *et al*, 2020). HDX mapping shows that CD53 and CD81 use similar parts of their C-D variable

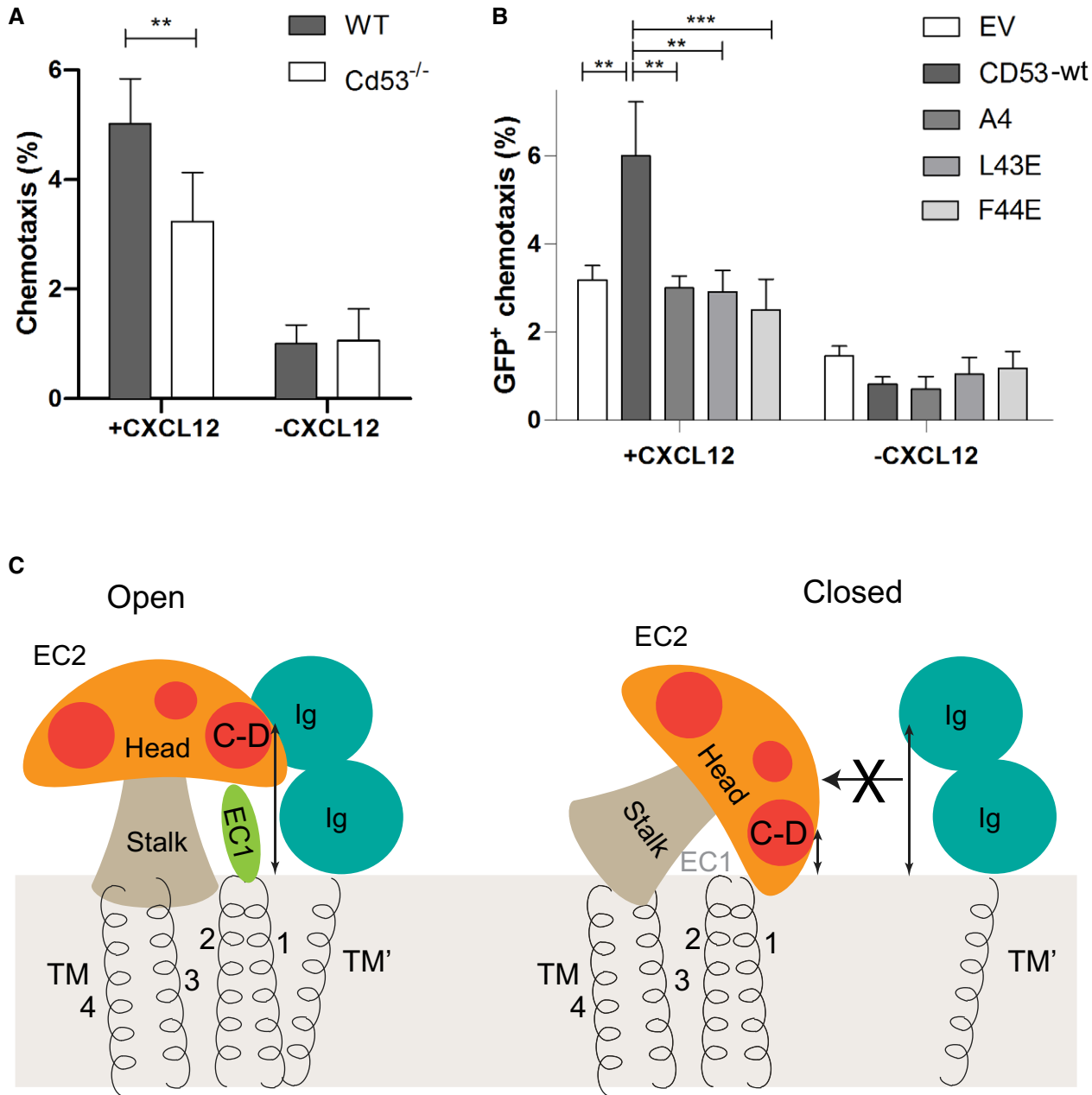


Figure 6. CD53 promotes the migration of pre-B cells and disruption of the CD53 open conformation impairs the migration.

A Migration of naïve Cd53^{-/-} cultured primary pre-B cells to 100 ng/ml CXCL12 compared to WT littermate controls ($n = 5$ mice per group) over three independent experiments. Bars and error bars represent mean \pm standard error of the mean. $**P < 0.01$ by two-way ANOVA.

B Migration of Cd53^{-/-} pre-B cells transduced with empty, control, or mutant constructs in response to CXCL12 gradient, 3 days after transduction ($n = 2-5$ mice per group) over two independent experiments. Bars and error bars represent mean \pm standard error of the mean. $**P < 0.01$ and $***P < 0.001$ by two-way ANOVA.

C Regulation of tetraspanin–partner interaction by open and closed conformational changes. The cartoon shows the mushroom fold of EC2 (stalk and head) and supporting interaction of EC1 (green). The spiral roots represent TMs. *Left*, Partner interaction at the open conformation requires EC2 in an exposed orientation and its C-D variable region at an above-membrane height (double arrow) matching that of the partner Ig domains. *Right*, Without the EC1 support (dimmed), changes in the EC2 orientation and C-D height prevent partner interactions in the closed conformation.

region to bind Ig-containing partners, whereas the binding regions on the Ig domains of CD2 and CD19 are distant from their membrane anchor (Fig 3). There is sufficient space for the bulky Ig domains to bind at the open conformation of CD81 or CD53 because their variable region has rotated away from the membrane plane. In contrast,

binding of Ig domains in the closed conformation would result in severe steric clashes with the membrane plane (Fig 3C and E). Similar conformational control may underlie interactions with various types of partners that bind to the variable region, such as many Ig superfamily proteins including CD2, CD4, CD8, EW1, and MHC I and

II in human cells. Likewise, binding of Ig-containing HCV envelope E2 protein relies on a critical residue, Phe186, on the D-loop (Higginbottom *et al*, 2000; Drummer *et al*, 2002). The CD81 D-loop also recruits clusters of CD81 and other tetraspanins on the plasma membrane (Homsy *et al*, 2014; Homsy & Lang, 2017). Similarly, interaction of integrins with CD151 depends on a QRD motif on its D-loop (Kazarov *et al*, 2002). The binding may also occur *in trans* between the oocyte CD9 and sperm IZUMO1 during fertilization; IZUMO1 binds to a SFQ motif on the CD9 D-loop (Zhu *et al*, 2002). Taken together, partner binding of different tetraspanins relies on specific residues in the EC2 variable region, especially the D-loop (Fig 3A). Moreover, the structural differences of the C-D region (Fig 2C) may largely control the partner specificity. Thus, the EC2 variation, which classifies tetraspanins into subgroups (Bonnet *et al*, 2019), may determine also the partner specificity of each individual tetraspanin. For example, the C8 subgroup of tetraspanins use their C–D variable region to interact specially with the ADAM family of metalloproteinases to assist their maturation (Haining *et al*, 2012; Lambrecht *et al*, 2018). Furthermore, these specific interactions may share a similar mechanism in that the EC2 rotation changes the accessibility of the variable region and its above-membrane height (Fig 6C) to control partner binding.

A major structural support for the open conformation is from the EC1–EC2 interaction. Previous phylogenomic analysis shows that the EC1 loop and EC2 head region have disproportionally high levels of new intron insertions, suggesting that both regions have evolved toward binding specific partners (Garcia-España *et al*, 2009). Changing the partner specificity by EC1 variation is likely through alternation of EC1–EC2 interaction. A previous low-resolution cryo-EM model of tetraspanin uroplakin predicts that EC2 folds on top of the EC1, albeit at the closed conformation (Min *et al*, 2006). Here, we found, however, that EC1 mutations disrupt the open conformation, thereby hindering CD81 from promoting accurate glycosylation of CD19 and hindering CD53 from promoting B-cell migration. Consistent with our findings is the previous demonstration that mutation of CD81 EC1 to polyalanine abolishes the *Plasmodium* infection (Yalaoui *et al*, 2008). Furthermore, the high-resolution structure of CD53 now provides direct evidence that EC1–EC2 interaction is required to stabilize the open conformation. EC1 binds at an EC2 groove formed between the stalk helices, and the sequence and structural variation of EC1 and the stalk helices may in turn change the EC2 orientation in different tetraspanins. For example, CD81 has a much longer EC1 than that of CD53, and their stalk helix A adopts different orientations (Fig 2C). Owing to these differences, MD modeling suggests that the open conformation of CD81 is different from that of CD53 (Fig 4A). Consequently, the molecular shape of CD81 and its accessible region for partner interaction also change. Similar variations in different tetraspanins may result in altered open conformations that contribute to the specificity for partner recognition.

Previous MD modeling predicted the dynamic motion of EC2 with several putative conformations (Umeda *et al*, 2020) that differ from the closed conformation observed in the CD81 and CD9 structures or the open conformation observed in the CD53 structure. In our MD simulation, however, the EC1-supported conformation of CD81 is quite stable (Fig 4B), probably because EC1 binds specifically into the hydrophobic groove of EC2. Without putting this specific and stabilizing interaction into consideration, previous MD

simulation may lead to many other conformations that appear to be more open or more closed; further experimental evidences are required to show whether these other conformational states truly exist. The EC1–EC2 interaction provides mutual stabilization between the transmembrane and EC2 domains, making their conformations nearly unaffected by the binding or release of cholesterol in our MD simulation (Fig 4A). Cholesterol release, however, was previously thought to cause dissociation of the TM pairs and trigger the open conformation; the disagreement between that and our conclusion is probably also because the previous modeling did not take EC1–EC2 interaction into consideration (Zimmerman *et al*, 2016). Consistently, structural comparisons suggest that the open conformation is independent of cholesterol releasing, because the CD81 structure with cholesterol and CD9 structure without cholesterol (Umeda *et al*, 2020) adopt nearly the same closed conformation. On the other hand, a monoolein molecule is bound at a similar position in CD9 and CD53 structures (Fig 2B), and yet CD53 adopts the open conformation. Because crystal structures generally capture a stable conformation, these structural observations suggest that, for CD53, the open conformation is more stable, and for CD9 and CD81, the closed conformation is more stable. In other words, the relative stability of open and closed conformations may vary in different tetraspanins.

Tetraspanins are emerging therapeutic targets for cancers, as multiple family members (e.g., CD81, CD53, CD9, CD151, TSPAN8, and CD37) have been implicated in tumor initiation, promotion, and/or metastasis (de Winde *et al*, 2017; Vences-Catalán & Levy, 2018; Bonnet *et al*, 2019; Vences-Catalán *et al*, 2019). CD81, for example, is expressed in a variety of solid tumors and hematopoietic malignancies, and loss of CD81 inhibits the invasion and metastasis of melanoma, breast, and lung tumor cells (Vences-Catalán *et al*, 2015). CD53 has been associated with hematopoietic malignancies, and its expression is upregulated in a variety of B-cell malignancies (Barrena *et al*, 2005), possibly protecting malignant B cells from apoptosis (Voehringer *et al*, 2000; Yunta & Lazo, 2003). In our current study, we observed reduced chemotaxis of CD53^{-/-} B cells toward CXCL12, a chemokine that supports both normal and leukemic B-cell trafficking and homing within the bone marrow (Möhle *et al*, 2000; Tokoyoda *et al*, 2004). As proper bone marrow niche localization is important for the growth and survival of leukemia cells, CD53 may be a useful therapeutic target for patients with B-cell malignancies. The crystal structure of CD53 contributes to our understanding of tetraspanin activity, and we predict that antibodies selectively blocking the open conformation of tetraspanins, including the support from EC1–EC2 interaction, may inhibit tetraspanin activity more specifically and afford a new therapeutic strategy for cancers involving upregulated tetraspanin expression.

Materials and Methods

Cloning and protein expression

The human CD53 cDNA (DNASU plasmid repository) was fused into a superfolder split GFP with a 10× His tag and cloned into a modified pPICZ-B expression vector (Invitrogen). To improve crystal diffraction, we made an Asn148Ala mutation to eliminate a

predicted glycosylation site, and Cys80Ala and Cys208Ala mutations to prevent palmitoylation. Site-specific mutagenesis was performed with QuikChange™ (Invitrogen). Nucleotide sequences were verified by DNA sequencing.

The human CD53 constructs were linearized and transformed into *Pichia pastoris* by electroporation. Transformants were selected by Zeocin resistance, and clones with the highest expression levels were selected by fluorescence-detection size-exclusion chromatography (Kawate & Gouaux, 2006). For large-scale protein expression, 1 l cell culture was grown in the BMG media (1% glycerol, 0.34% yeast nitrogen base, 1% ammonium sulfate, 0.4 µg/ml biotin, and 100 mM potassium phosphate pH 6.0) at 30°C for 20 h. The growth media were exchanged to the media without glycerol, and protein expression was induced with 0.7% methanol for 2 days at 25°C. The cells were harvested by centrifugation and flash-frozen in liquid nitrogen.

Protein purification

Frozen *Pichia* cells (20 g) were applied to a ball mill (Retsch) to break the cell wall. The cell membrane was subsequently solubilized in a buffer containing 2% DDM, 150 mM NaCl, 100 mM Tris-HCl pH 8.0, 10 µg/ml DNase I, and protease inhibitor cocktail. After stirring at 4°C for 3 h, the suspension was centrifuged at 20,000 g for 45 min. Subsequently, the supernatant was incubated with TALON metal-affinity resin (Clontech) for 3 h at 4°C. The resin was collected on a gravity-flow column and washed with 20 mM imidazole, 2 mM DDM, 150 mM NaCl, and 20 mM Tris pH 8.0. The protein was eluted with 250 mM imidazole, 1 mM DDM, 150 mM NaCl, and 20 mM Tris pH 8.0. The protein was subsequently concentrated and applied to Superdex 200 for size-exclusion chromatography (SEC) in a buffer containing 0.05% lauryl maltose neopentyl glycol (LMNG), 150 mM NaCl, and 20 mM Tris pH 8.0. The purified protein was concentrated to ~66 mg/ml and used immediately for crystallization.

Crystallization and data collection

Purified CD53 was reconstituted into lipidic cubic phase (LCP) by thorough mixing with monoolein at a 2:3 ratio (v/v) using a coupled syringe. The reconstituted protein (100 nl) was dispensed onto a glass plate by a Gryphon LCP robot (Art Robbins Instruments) and overlaid with 800 nl of precipitant solution containing 25–30% PEG400, 0.1 M KH₂PO₄, and 0.1 M MES pH 6.0. The LCP plates were incubated at 22°C. Crystals appeared overnight and grew to an optimal size after 1 week. The crystals were harvested from the mesophase bolus and flash-frozen in liquid nitrogen. The data were collected with a microfocus beam and a PILATUS detector at the ID-24 beamlines of Advanced Photon Source.

Structure determination

Molecular replacement (MR) was conducted with Phaser (McCoy *et al.*, 2007) using the fused sfGFP (Pédélecq *et al.*, 2006) as the search model (PDB code 2B3P). This MR model was rigid-body refined with REFMAC (Murshudov *et al.*, 1997). The partial model phases were improved by solvent flattening and two-fold averaging using program PARROT (Cowtan, 2010) and DM (Cowtan, 1994).

The density modified maps were sufficient for automatic model building of the CD53 region (~80–90% completeness) by the BUCCANEER software (Cowtan, 2010). The models were manually built into complete and refined against the data by refinement programs installed in the PHENIX suites (Afonine *et al.*, 2012).

Protein purification for HDX-MS

The proteins used for HDX-MS analyses were EC2 domain of CD53 (residues 107–181), EC2 domain of CD81 (residues 112–202), Ig domains of CD2 (residues 1–205), and Ig domains of CD19 (residues 1–277). These proteins were tagged with an N-terminal signal peptide (MGILPSPGMPALLSLVLSVLLMGCVVA) and a C-terminal PreScission protease site (LEVLFQ/GP) followed by a GFP with 10× His tag (C-GFP-His). The coding DNA constructs were cloned into a modified BacMam expression vector (Goehring *et al.*, 2014). The plasmids were transformed into DH10Bac cells to produce bacmids, which were subsequently transfected into Sf9 cells by using Cellfectin II (Thermo) for baculovirus production. The P2 virus was used to transfect HEK293 GnT1⁻ suspension cells that were grown in FreeStyle media at 37°C. After 8–12 h infection, 10 mM sodium butyrate was added and the temperature was adjusted to 30°C. The culture media containing the secreted proteins were collected after 72 h of baculovirus transfection.

The media were diluted in 150 mM NaCl and 50 mM Tris pH 8.0 and incubated with TALON metal-affinity resin. The resin was collected on a gravity-flow column and washed with the same buffer containing 20 mM imidazole. The resin-bound protein was digested with 20 µg/ml PreScission protease to remove the C-GFP-10xHis tag. The eluent was further purified through a Superdex 200 column in a buffer containing 150 mM NaCl and 20 mM Tris pH 8.0. The purified proteins were concentrated to 300 µM and stored at –80°C before HDX-MS analyses. Prior to HDX, CD19 was deglycosylated with PNGase F at 4°C overnight.

HDX-MS analyses

HDX experiments were performed in triplicate at 4°C with exchange times of 10, 30, 60, 900, 3,600, 7,200, and 14,400 s. The experiments were performed either manually (CD53, CD81 and CD19) or with LEAP automation system (CD53 and CD2). The bound state of each protein was generated by mixing with higher molar ratio (1:2 or 1:3) of its partner protein and incubating at 4°C overnight to allow equilibration. The protein solutions at unbound and bound states were diluted into D₂O buffer (80–90% D) containing 150 mM NaCl and 20 mM Tris pH 8.0. The HDX was quenched at 25°C for 60 s in a solution (2:3 v/v) containing 4 M urea and 200 mM tris(2-carboxyethyl)phosphine hydrochloride (TCEP); the solution was adjusted to pH 2.5 to minimize back exchange. CD2 required 500 mM TCEP for a more complete disulfide reduction. The quenched mixture was submitted into a custom-packed pepsin column for digestion at a flow rate of 200 µl/min in 0.1% trifluoro acetic acid. The digested peptide was captured by a ZORBAX Eclipse XDB C8 column (2.1 × 15 mm, Agilent). After 3 min of digesting and desalting, the flow was switched to a liquid chromatography gradient using water as phase A and 80% acetonitrile as phase B (both containing 0.1% formic acid). The digested peptides were further separated on a C-18 column (Waters) prior to MS analysis. The data were collected by a

Quadrupole time-of-flight mass spectrometer (Bruker MaXis). All HDX procedures and HPLC separations, besides the pepsin digestion, were conducted in an ice-water bath to minimize back exchange.

Peptide mapping was by MS/MS, and data were identified by Byonic and processed with Byologic (Protein Metrics). Peptide lists together with the raw data were submitted into HDEaminer (Sierra Analytics) for analysis. Mapping for all four proteins gave 100% sequence coverages. HDX-MS reached full coverage of CD81, 70% coverage of CD53 and CD2, and 63% coverage of CD19 due to glycosylation or high β -sheet content. Most part of CD2 shows limited deuterium uptake under unbound and bound states, owing to the extensive hydrogen bonding in its β -sheet-rich structure.

Molecular docking

Information-driven docking was performed using the HADDOCK2.2 webserver (Van Zundert *et al*, 2016). For the docking between CD53 EC2 and CD2 Ig, the crystal structures of CD53 (Fig 1A) and CD2 Ig (PDB code 1HNF) were used. According to the HDX-MS results (Fig 3B), residues 152–167 in CD53 and residues 124–128 in CD2 were specified as the binding regions (“active” residues) for the information-driven docking in HADDOCK. The surrounding surface residues (“passive” residues) were defined automatically by the program. The docking model was selected from clusters with low HADDOCK score and favorable membrane orientation (C-terminal of CD2 Ig domain close to membrane). Similarly, the docking between CD81 EC2 and CD19 Ig domains was performed by using the crystal structures of CD81 (PDB code 5TCX) and CD19 Ig (PDB code 6AL5); residues 171–185 in CD81 and 182–196 in CD19 were defined as the binding regions based on the HDX-MS results (Fig 3D).

Modeling of CD81 in open conformation and CD53 in closed conformation

To model the open conformation of CD81, we first used HADDOCK to generate a docking model between the entire EC1 (residues 38–54) and EC2 regions (116–200). This docking model was superimposed by EC2 domain onto the CD53 structure at open conformation. To accommodate the longer EC1 in CD81, orientation of the EC1-EC2 docking model was manually adjusted. The docking model was subsequently linked to transmembrane domain of CD81, which was superimposed also onto the CD53 structure, to generate a full-length CD81 model at the open conformation. This initial model was inserted into a POPC bilayer by using CHARMM-GUI (Vanommeslaeghe *et al*, 2010). Molecular dynamics simulation of this system was performed with GROMACS MD simulation package (Van Der Spoel *et al*, 2005) with CHARMM36m force field (Huang *et al*, 2017). For MD simulation, the system was first energy minimized using a steepest descent algorithm with a 0.01-nm step size and a 1.2-nm neighbor-list cutoff distance for Coulomb and Van der Waals interactions until the maximum force on any atom in the system fell below 1,000 kJ/mol/nm. The system was then equilibrated for 0.25 ns with a 0.001-fs time step and a Berendsen thermostat to hold the system temperature at 303.15 K. A Verlet cutoff scheme was used for the neighbor list. Particle mesh Ewald was used for the Coulomb interactions. Parrinello–Rahman barostat and velocity-rescaling thermostat were used for the 1 μ s MD simulation.

The closed conformation of CD53 was generated from homology modeling, using the Swiss Model Server (Schwede *et al*, 2003) with the CD81 structure (PDB: 5TCX) as the template.

Generation of CD81-knockout 293T cells

The pre-validated sgRNA coding sequence of CD81 was cloned into all-in-one vector containing enhanced specificity SpCas9 (GenScript). The plasmid (3 μ g) was transfected into HEK293T cells on a 6-well plate by using Lipofectamine 3000. After 2 days, the cells were transferred to 96-well plates and diluted. Single cell clones were isolated after 10 days. The CD81 knockouts were identified by Western blot with a CD81 antibody (Thermo 17-0819-42).

CD19 maturation analyses

The coding sequence of human CD81 with a V5-tag and CD19 with a FLAG-tag at C-terminus was cloned into a pCMV6-Entry vector. Site-directed mutagenesis of CD81 was performed by QuikChange™, and the nucleotide sequences of all the constructs were verified by DNA sequencing. The CD81 and CD19 constructs were transfected into the CD81-knockout HEK-293T cells grown in DMEM and 10% FBS. After 48 h of transfection, cells were lysed for 30 min in a buffer containing 2% DDM, 150 mM NaCl, 20 mM Tris-HCl pH 7.5, and protease inhibitor cocktail. The cell lysates were centrifuged at 20,000 g for 20 min at 4°C. The supernatant was boiled with loading buffer before applying to SDS-PAGE. Western blot was performed with anti-V5 (Thermo MA532053), anti-actin (Santa Cruz sc-1616 HRP), or anti-FLAG M2 antibodies (Sigma F2555).

For the deglycosylation of CD19 species, supernatant of the cell lysate was digested with PNGase F or Endo H (NEB) following the manufacturer's instructions. Trypsin digestion of CD19 (Invitrogen) was performed on intact cells, and the incubation was at 37°C for different times.

Mice

Cd53^{-/-} mice were generated via CRISPR/Cas9 technology and maintained on a C57BL/6J background, as previously described (Greenberg *et al*, 2020), with wild-type (WT) C57BL/6J mice used as controls. Sex-matched 6- to 8-week-old mice were used for each experiment in accordance with the guidelines of the Washington University Animal Studies Committee.

Retroviral transduction

The coding sequence of *Mus musculus* CD53 with a C-terminal GFP tag was cloned into a MigR1 vector. The vectors containing wild-type and mutant CD53 were transfected into Platinum-E cells (CellBio Labs) using polyethylenimine. Viral supernatants were collected 48 h after transfection.

Primary pre-B-cell (B220⁺CD19⁻CD43⁺) cultures were generated by culturing bone marrow from 6- to 8-week-old Cd53^{-/-} or C57BL/6J mice. The cells were grown in DMEM/FBS media with 5 ng/ml IL-7 (PeproTech) for 7–10 days until the cell density reached 2×10^6 cells/ml (Soodgupta *et al*, 2019). The cultures were > 90% pre-B cells (B220⁺ CD19⁺ CD43^{mid}) in both WT and CD53^{-/-} cultures. The purity of cell population was assessed by flow cytometry with

the staining of pre-B cells by all three antibodies to confirm that the cells used were phenotypic pre-B cells.

For viral transduction, 2 ml viral supernatants were applied to RetroNectin coated 6-well plates (Takara) and centrifuged at 2,500 g for 90 min at 32°C. Supernatants were subsequently removed, and pre-B-cell cultures were added and centrifuged at 185 g for 7 min. The transduced pre-B cells were maintained in the same media with 5 ng/ml IL-7 and cultured for 2–3 days until GFP signal was detected by flow cytometry.

Transwell migration assay

A total of 0.5×10^6 cells/100 μ l GFP⁺ pre-B cells (transduction efficiency confirmed by flow cytometry) were placed in the upper compartment of a transwell chamber (5 μ m pore size, Corning), and 600 μ l of pre-warmed IL-7 medium + 100 ng/ml CXCL12 (Pepro-Tech) in the well below. Cells were cultured at 37°C in a 5% CO₂ humidified incubator for 2 h. Transwells were removed, and migrated cells were measured by fixed-volume flow cytometry. Percent migration was recorded as [(# of cells migrated)/(# of cells input)] \times 100.

Data availability

Structure factors and coordinates have been deposited in the Protein Data Bank with identification numbers PDB: 6WVG.

Expanded View for this article is available online.

Acknowledgements

W.L. is supported by W. M. Keck Foundation (Forefront of Science Award), NHLBI (R01 HL121718), and NEI (R21 EY028705). L.S. and W.L. are supported by Children's Discovery Institute (MCII 2020-854). T.E. is supported by NIAID (R01 AI130152) and Leukemia & Lymphoma Society (Scholar Award). The HDX-MS are supported by NIGMS (P41 GM103422) to M.L.G. and by NIGMS (R01 GM131008) to M.L.G. and W.L..

Author contributions

WL and YY conceived the project and designed the experiments. YY obtained the crystals, and WL determined the structure. SL assisted the crystallization. YY generated the docking models, and FZ performed the MD simulation. YY investigated the CD19 maturation with the assist from LF, GS, and WL. YY and PH purified the proteins for HDX-MS, and XRL performed the HDX-MS under the guidance of MLG. TE and YY generated the retrovirus. ZJG and LGS generated the mouse strains and performed the migration assay. WL wrote the paper with input from YY, LGS, MLG, ZJG, and XRL.

Conflict of interest

The authors declare that they have no conflict of interest.

References

Afonine PV, Grosse-Kunstleve RW, Echols N, Headd JJ, Moriarty NW, Mustyakimov M, Terwilliger TC, Urzhumtsev A, Zwart PH, Adams PD (2012) Towards automated crystallographic structure refinement with phenix.refine. *Acta Crystallogr D Biol Crystallogr* 68: 352–367

Bagashev A, Sotillo E, Tang C-HA, Black KL, Perazzelli J, Seeholzer SH, Argon Y, Barrett DM, Grupp SA, Hu C-CA et al (2018) CD19 alterations emerging after CD19-directed immunotherapy cause retention of the misfolded protein in the endoplasmic reticulum. *Mol Cell Biol* 38: e00383–00318

Barrena S, Almeida J, Yunta M, López A, Fernández-Mosteirín N, Giralt M, Romero M, Perdiguer L, Delgado M, Orfao A et al (2005) Aberrant expression of tetraspanin molecules in B-cell chronic lymphoproliferative disorders and its correlation with normal B-cell maturation. *Leukemia* 19: 1376–1383

Beckwith KA, Byrd JC, Muthusamy N (2015) Tetraspanins as therapeutic targets in hematological malignancy: a concise review. *Front Physiol* 6: 91

Bell GM, Seaman WE, Niemi EC, Imboden JB (1992) The OX-44 molecule couples to signaling pathways and is associated with CD2 on rat T lymphocytes and a natural killer cell line. *J Exp Med* 175: 527–536

Bonnet M, Maisonia-Beset A, Zhu Y, Witkowski T, Roche G, Boucheix C, Greco C, Degoul F (2019) Targeting the tetraspanins with monoclonal antibodies in oncology: focus on tspan8/Co-029. *Cancers* 11: E179

Braig F, Brandt A, Goebeler M, Tony HP, Kurze AK, Nollau P, Bumm T, Böttcher S, Bargou RC, Binder M (2017) Resistance to anti-CD19/CD3 BiTE in acute lymphoblastic leukemia may be mediated by disrupted CD19 membrane trafficking. *Blood* 129: 100–104

Charrin S, le Naour F, Silvie O, Milhiet P-E, Boucheix C, Rubinstein E (2009) Lateral organization of membrane proteins: tetraspanins spin their web. *Biochem J* 420: 133–154

Charrin S, Jouannet S, Boucheix C, Rubinstein E (2014) Tetraspanins at a glance. *J Cell Sci* 127: 3641–3648

Cowtan KD (1994) “dm”: an automated procedure for phase improvement by density modification. *Joint CCP4 ESF-EACBM Newslett Protein Crystallogr* 31: 34–38

Cowtan KD (2010) Recent developments in classical density modification. *Acta Crystallogr D Biol Crystallogr* 66: 470–478

Demaria MC, Yeung L, Peeters R, Wee JL, Mihaljcic M, Jones EL, Nasa Z, Alderuccio F, Hall P, Smith BC et al (2020) Tetraspanin CD53 promotes lymphocyte recirculation by stabilizing L-selectin surface expression. *iScience* 23: 101104

Drummer HE, Wilson KA, Pountourios P (2002) Identification of the hepatitis C virus E2 glycoprotein binding site on the large extracellular loop of CD81. *J Virol* 76: 11143–11147

Fischer J, Paret C, El Malki K, Alt F, Wingerter A, Neu MA, Kron B, Russo A, Lehmann N, Roth L et al (2017) CD19 isoforms enabling resistance to CART-19 immunotherapy are expressed in B-ALL patients at initial diagnosis. *J Immunother* 40: 187–195

García-España A, Mares R, Sun TT, DeSalle R (2009) Intron evolution: testing hypotheses of intron evolution using the phylogenomics of tetraspanins. *PLoS ONE* 4: e4680

Geisert EE, Williams RW, Geisert GR, Fan L, Asbury AM, Maecker HT, Deng J, Levy S (2002) Increased brain size and glial cell number in CD81-null mice. *J Comp Neurol* 453: 22–32

Goehring A, Lee CH, Wang KH, Michel JC, Claxton DP, Bacongus I, Althoff T, Fischer S, Garcia KC, Gouaux E (2014) Screening and large-scale expression of membrane proteins in mammalian cells for structural studies. *Nat Protoc* 9: 2574–2585

Greenberg ZJ, Monlish DA, Barnett RL, Yang Y, Shen G, Li W, Bednarski JJ, Schuettpeiz LG (2020) The tetraspanin CD53 regulates early B cell development by promoting IL-7R signaling. *J Immunol* 204: 58–67

Haining EJ, Yang J, Bailey RL, Khan K, Collier R, Tsai S, Watson SP, Frampton J, Garcia P, Tomlinson MG (2012) The TspanC8 subgroup of tetraspanins

- interacts with a disintegrin and metalloprotease 10 (ADAM10) and regulates its maturation and cell surface expression. *J Biol Chem* 287: 39753–39765
- Higginbottom A, Quinn ER, Kuo CC, Flint M, Wilson LH, Bianchi E, Nicosia A, Monk PN, McKeating JA, Levy S (2000) Identification of amino acid residues in CD81 critical for interaction with hepatitis C virus envelope glycoprotein E2. *J Virol* 74: 3642–3649
- Homsy Y, Schloetel JG, Scheffer KD, Schmidt TH, Destainville N, Florin L, Lang T (2014) The extracellular δ -domain is essential for the formation of CD81 tetraspanin webs. *Biophys J* 107: 100–113
- Homsy Y, Lang T (2017) The specificity of homomeric clustering of CD81 is mediated by its δ -loop. *FEBS Open Biol* 7: 274–283
- Huang S, Yuan S, Dong M, Su J, Yu C, Shen Y, Xie X, Yu Y, Yu X, Chen S et al (2005) The phylogenetic analysis of tetraspanins projects the evolution of cell-cell interactions from unicellular to multicellular organisms. *Genomics* 86: 674–684
- Huang J, Rauscher S, Nawrocki G, Ran T, Feig M, de Groot BL, Grubmuller H, MacKerell AD Jr (2017) CHARMM36m: an improved force field for folded and intrinsically disordered proteins. *Nat Methods* 14: 71–73
- Jia X, Schulte L, Loukas A, Pickering D, Pearson M, Mobli M, Jones A, Rosengren KJ, Daly NL, Gobert GN et al (2014) Solution structure, membrane interactions, and protein binding partners of the tetraspanin Sm-TSP-2, a vaccine antigen from the human blood fluke schistosoma mansoni. *J Biol Chem* 289: 7151–7163
- Kawate T, Gouaux E (2006) Fluorescence-detection size-exclusion chromatography for precrystallization screening of integral membrane proteins. *Structure* 14: 673–681
- Kazarov AR, Yang X, Stipp CS, Sehgal B, Hemler ME (2002) An extracellular site on tetraspanin CD151 determines $\alpha 3$ and $\alpha 6$ integrin-dependent cellular morphology. *J Cell Biol* 158: 1299–1309
- Kitadokoro K, Bordo D, Galli G, Petracca R, Falugi F, Abrignani S, Grandi G, Bolognesi M (2001) CD81 extracellular domain 3D structure: insight into the tetraspanin superfamily structural motifs. *EMBO J* 20: 12–18
- Lambrecht BN, Vanderkerken M, Hammad H (2018) The emerging role of ADAM metalloproteinases in immunity. *Nat Rev Immunol* 18: 745–758
- Maecker HT, Levy S (1997) Normal lymphocyte development but delayed humoral immune response in CD81-null mice. *J Exp Med* 185: 1505–1510
- McCoy AJ, Grosse-Kunstleve RW, Adams PD, Winn MD, Storoni LC, Read RJ (2007) Phaser crystallographic software. *J Appl Crystallogr* 40: 658–674
- Min G, Wang H, Sun TT, Kong XP (2006) Structural basis for tetraspanin functions as revealed by the cryo-EM structure of uroplakin complexes at 6-Å resolution. *J Cell Biol* 173: 975–983
- Möhle R, Schittenhelm M, Failenschmid C, Bautz F, Kratz-Albers K, Serve H, Brugger W, Kanz L (2000) Functional response of leukaemic blasts to stromal cell-derived factor-1 correlates with preferential expression of the chemokine receptor CXCR4 in acute myelomonocytic and lymphoblastic leukaemia. *Br J Haematol* 110: 563–572
- Mollinedo F, Fontan G, Barasoain I, Lazo PA (1997) Recurrent infectious diseases in human CD53 deficiency. *Clin Diagn Lab Immunol* 4: 229–231
- Murshudov GN, Vagin AA, Dodson EJ (1997) Refinement of macromolecular structures by the maximum-likelihood method. *Acta Crystallogr D Biol Crystallogr* 53: 240–255
- Omae Y, Toyo-Oka L, Yanai H, Nedsuwan S, Wattanapokayakit S, Satproedprai N, Smittipat N, Palittapongarnpim P, Sawanpanyalert P, Inunchot W et al (2017) Pathogen lineage-based genome-wide association study identified CD53 as susceptible locus in tuberculosis. *J Hum Genet* 62: 1015–1022
- Park JH, Geyer MB, Brentjens RJ (2016) CD19-targeted CAR T-cell therapeutics for hematologic malignancies: interpreting clinical outcomes to date. *Blood* 127: 3312–3320
- Pédélecq JD, Cabantous S, Tran T, Terwilliger TC, Waldo GS (2006) Engineering and characterization of a superfolder green fluorescent protein. *Nat Biotechnol* 24: 79–88
- Rajesh S, Sridhar P, Tews BA, Feneant L, Cocquerel L, Ward DG, Berditchevski F, Overduin M (2012) Structural basis of ligand interactions of the large extracellular domain of tetraspanin CD81. *J Virol* 86: 9606–9616
- Schwede T, Kopp J, Guex N, Peitsch MC (2003) SWISS-MODEL: an automated protein homology-modeling server. *Nucleic Acids Res* 31: 3381–3385
- Seigneuret M, Delaguillaumie A, Lagaudrière-Gesbert C, Conjeaud H (2001) Structure of the tetraspanin main extracellular domain: a partially conserved fold with a structurally variable domain insertion. *J Biol Chem* 276: 40055–40064
- Seigneuret M (2006) Complete predicted three-dimensional structure of the facilitator transmembrane protein and hepatitis C virus receptor CD81: conserved and variable structural domains in the tetraspanin superfamily. *Biophys J* 90: 212–227
- Shoham T, Rajapaksa R, Boucheix C, Rubinstein E, Poe JC, Tedder TF, Levy S (2003) The tetraspanin CD81 regulates the expression of CD19 during B cell development in a postendoplasmic reticulum compartment. *J Immunol* 171: 4062–4072
- Shoham T, Rajapaksa R, Kuo CC, Haimovich J, Levy S (2006) Building of the tetraspanin web: distinct structural domains of CD81 function in different cellular compartments. *Mol Cell Biol* 26: 1373–1385
- Soodgupta D, White LS, Yang W, Johnston R, Andrews JM, Kohyama M, Murphy KM, Mosammaparast N, Payton JE, Bednarski JJ (2019) RAG-Mediated DNA breaks attenuate PU.1 activity in early B cells through activation of a SPIC-BCLAF1 complex. *Cell Rep* 29: 829–843
- Sutovsky P (2009) Sperm-egg adhesion and fusion in mammals. *Expert Rev Mol Med* 11: e11
- Termini CM, Gillette JM (2017) Tetraspanins function as regulators of cellular signaling. *Front Cell Dev Biol* 5: 34
- Tokoyoda K, Egawa T, Sugiyama T, Choi BI, Nagasawa T (2004) Cellular niches controlling B lymphocyte behavior within bone marrow during development. *Immunity* 20: 707–718
- Umeda R, Satouh Y, Takemoto M, Nakada-Nakura Y, Liu K, Yokoyama T, Shirouzu M, Iwata S, Nomura N, Sato K et al (2020) Structural insights into tetraspanin CD9 function. *Nat Commun* 11: 1606
- Van Der Spoel D, Lindahl E, Hess B, Groenhof G, Mark AE, Berendsen HJC (2005) GROMACS: fast, flexible, and free. *J Comput Chem* 26: 1701–1718
- Van Deventer SJ, Dunlock VME, Van Spriel AB (2017) Molecular interactions shaping the tetraspanin web. *Biochem Soc Trans* 45: 741–750
- Vanommeslaeghe K, Hatcher E, Acharya C, Kundu S, Zhong S, Shim J, Darian E, Guvench O, Lopes P, Vorobyov I et al (2010) CHARMM general force field: a force field for drug-like molecules compatible with the CHARMM all-atom additive biological force fields. *J Comput Chem* 31: 671–690
- Velasquez MP, Gottschalk S (2017) Targeting CD19: the good, the bad, and CD81. *Blood* 129: 9–10
- Vences-Catalán F, Rajapaksa R, Srivastava MK, Marabelle A, Kuo CC, Levy R, Levy S (2015) Tetraspanin CD81 promotes tumor growth and metastasis by modulating the functions of T regulatory and myeloid-derived suppressor cells. *Can Res* 75: 4517–4526
- Vences-Catalán F, Levy S (2018) Immune targeting of tetraspanins involved in cell invasion and metastasis. *Front Immunol* 9: 1277
- Vences-Catalán F, Kuo CC, Rajapaksa R, Duault C, Andor N, Czerwinski DK, Levy R, Levy S (2019) CD81 is a novel immunotherapeutic target for B cell lymphoma. *J Exp Med* 216: 1497–1508
- Voehringer DW, Hirschberg DL, Xiao J, Lu Q, Roederer M, Lock CB, Herzenberg LA, Steinman L, Herzenberg LA (2000) Gene microarray identification of

- redox and mitochondrial elements that control resistance or sensitivity to apoptosis. *Proc Natl Acad Sci USA* 97: 2680–2685
- Wang K, Wei G, Liu D (2012) CD19: a biomarker for B cell development, lymphoma diagnosis and therapy. *Exp Hematol Oncol* 1: 36
- de Winde CM, Elfrink S, van Spriël AB (2017) Novel insights into membrane targeting of B cell lymphoma. *Trends Cancer* 3: 442–453
- Yalaoui S, Zougbedé S, Charrin S, Silvie O, Arduise C, Farhati K, Boucheix C, Mazier D, Rubinstein E, Froissard P (2008) Hepatocyte permissiveness to *Plasmodium* infection is conveyed by a short and structurally conserved region of the CD81 large extracellular domain. *PLoS Pathog* 4: e1000010
- Yeung L, Hickey MJ, Wright MD (2018) The many and varied roles of tetraspanins in immune cell recruitment and migration. *Front Immunol* 18: 1644
- Yunta M, Lazo PA (2003) Apoptosis protection and survival signal by the CD53 tetraspanin antigen. *Oncogene* 22: 1219–1224
- Zhu GZ, Miller BJ, Boucheix C, Rubinstein E, Liu CC, Hynes RO, Myles DG, Primakoff P (2002) Residues SFQ (173-175) in the large extracellular loop of CD9 are required for gamete fusion. *Development* 129: 1995–2002
- Zimmerman B, Kelly B, McMillan BJ, Seegar TCM, Dror RO, Kruse AC, Blacklow SC (2016) Crystal structure of a full-length human tetraspanin reveals a cholesterol-binding pocket. *Cell* 167: 1041–1051
- Zuidscherwoude M, Dunlock VME, Van Den Bogaart G, Van Deventer SJ, Van Der Schaaf A, Van Oostrum J, Goedhart J, In't Hout J, Hämmerling GJ, Tanaka S et al (2017) Tetraspanin microdomains control localized protein kinase C signaling in B cells. *Sci Signal* 10: 478